7th International Conference
on
Wind Turbine Noise
Rotterdam 2-5 May 2017

Wind Turbine Sound Prediction: Modelling and Case Study on the Effect of Blade Elasticity

L. Schorle University of Siegen, 57068 Siegen, Germany
E-Mail: leonard.schorle@uni-siegen.de

T. Carolus University of Siegen , 57068 Siegen, Germany
E-Mail: thomas.carolus@uni-siegen.de

S. Erbslöh Senvion SE, 24783 Osterrönfeld, Germany
E-Mail: sascha.erbsloeh@senvion.com

Abstract

Sound prediction tools for wind turbines are essential in the initial phase of planning in order to meet regulatory immission standards and for estimating the effect of modifications during turbine development on the sound immitted at relevant monitoring points. They can be classified in three methodologically different categories: Empirical one-equation models, semi-analytical models and computational aeroacoustics methods. Objectives of this contribution are to compile and compare selected aeroacoustic semi-analytical wind turbine sound prediction models available in the open literature, and conduct a first case study.

The general structure of all semi-analytical models is found to be similar: A combination of sub-models for the elementary sound sources on the blades and a sound propagation model from the sources to the listener. Trailing edge sound is identified as the dominant source in state-of-the art wind turbines. However, the sub-models for this elementary sound source found in the literature vary substantially. Combining selected sub-models, a preliminary own wind turbine sound prediction model was compiled and encoded, yielding the acoustic footprint of the turbine on ground level and the swishing character of the wind turbine sound.

HOWE's sound source directivity function seems to yield results, that match best with experimental results from literature. Also, from principle considerations ROZENBERG's approach for the convective amplification factor, taking into account the motion of the elementary sound sources, seems to be the most consistent.

In a first case study, the effect of delocalisation of elementary sound sources along the blades and a modification of the local angle of attack due to the flexibility of the blade has been studied. As a preliminary result, the effect of blade elasticity on the acoustic emission of a complete wind turbine rotor seems to be small when comparing to a rigid rotor.

It is important to note that so far the atmospheric attenuation, refraction and ground effects have not been taken into account - this remains for future studies and may affect these results.

Nomenclature

Symbols

A, B	correction factors	dB
C	chord length of the airfoil	m
CA	convective amplification factor	
D	directivity function of the trailing edge sound	
f	acoustic frequency of the source	Hz
f'	shifted acoustic frequency at the observer	Hz
K_1, K_2, ΔK_1	correction factors	dB
L	spanwise length of the blade segment	m
M	free Mach number	
m	total amount of sound sources	
n	exponent in the convective amplification equation	
$OASPL$	overall sound pressure level (over all frequencies)	dB
p_{ref}	reference value for the sound pressure ($2 \cdot 10^{-5}$)	Pa
r	distance between the source and the observer	m
r_{Obs}	radial distance between the observer and the WT foot	m
R	radial position of a sound source on the rotor blade	m
SPL	sound pressure level	dB
S_{pp}	power spectral density (sound pressure) at the source	Pa^2/Hz
S'_{pp}	power spectral density (sound pressure) at the observer	Pa^2/Hz
St	Strouhal number	
t	source time	s
t'	observer time	s
T	time period of one rotor revolution	s
U	free-stream velocity	m/s
U_W	inflow velocity of the wind in the rotor plane	m/s
v_r	circumferential speed in the rotation plane	m/s
W_∞	relative inflow speed in the rotation plane	m/s
α	angle of attack	°
β_∞	free inflow angle	°
β_{cone}	cone angle	°
γ	stagger angle	°
δ^*	boundary layer displacement thickness	m
ζ	observer angle (ζ = 0° in front of the wind turbine)	°
λ	acoustic wave length	m
σ_R	rotor twist angle	°
σ_T	elastic torsion angle	°
σ_P	pitch angle	°
Γ_W	tilt angle	°
Ψ	azimuth angle	°
β, γ_R, Θ_H, Φ_A, Θ_A, Φ_H	directivity function angles	°

Further indices

am	Amplitude modulation
eq	equivalent

norm	normalized with respect to the position directly in front of the WT
p	pressure side of the airfoil
ref	reference case with r = 1 m and D = 1
s	suction side of the airfoil
SO	source and observer
TOT	contributions from suction and pressure side (for an elementary source)
total	total sound pressure (summation over all elementary sources)
1/3	1/3 octave band spectrum

1. Introduction

The sound emitted by wind turbines is a relevant criterion for onshore and potentially even offshore installations. Sound prediction tools are essential in the initial phase of planning a wind turbine installation in order to meet regulatory immission standards and, more recently, for an early assessment of perceptual reaction from listeners as addressed e.g. by EGGENSCHWILER et al. [1]. They also may allow for estimating the effect of modifications of the turbine during the phase of technical development. For instance, how does a delocalisation of sound radiating portions of the blade due to the elasticity of the blades affect the turbine's overall far field sound pressure at relevant observer points? Or modification of the details of the flow around the blade e.g. by means of trailing edge suction [2] or blowing [3]. Or the increasingly popular edge serration [4] which intervene in the sound scattering process.

There is a variety of sound sources potentially relevant in modern wind turbines. Two principal categories may be distinguished: (i) mechanic sound sources like the gear box or the generator, and (ii) aeroacoustic sound sources like the trailing edge, inflow or tip sound source. According to OERLEMANS et al. [5] who did an extensive acoustic field measurement on a wind turbine as well as numerous other researchers in the past, trailing edge sound is regarded as the dominant aeroacoustic sound source in modern wind turbines

The phenomena, relevant for an observer perceiving turbine sound, are illustrated schematically in **Fig. 1**: Starting points are a number of elementary sound sources of given strength and directivity distributed at the blade surfaces. The superposition of all elementary sound sources with their instantaneous orientation and motion with respect to an observer forms the time dependent far field sound pressure. While propagating, sound rays from these sources are refracted and damped in the atmosphere and reflected on the ground.

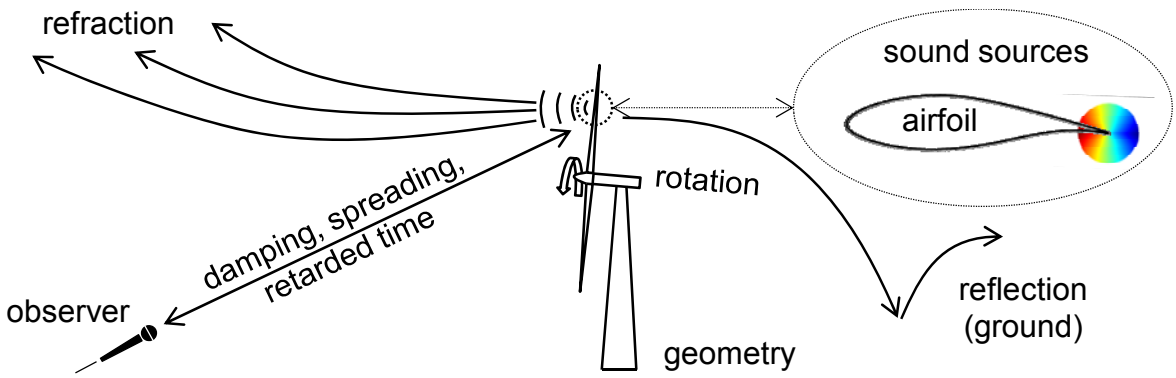

Figure 1: Wind turbine sound: Possible influencing factors on the sound immission at an observer-position

According to LOWSON [6], sound prediction methods for wind turbines can be classified in three methodologically different categories: (i) empirical one equation models as e.g. from LIPS [7] or in the German standard DIN EN 61400-11 [8], that are merely based on basic parameters of the wind turbine, (ii) semi-analytical models, which model different sound source mechanisms, and (iii) methods which are based on a full description of the turbine's geometry and flow, so-called computational aeroacoustics methods (CAA). State-of-the-art semi-analytical sound prediction models contains a number of steps:

- Segmentation of blades into a number of blade elements
- Based on sound source models: computation of sound source data (source strength and directivity for each blade element)
- Calculation of propagation of each elementary sound source to listener position, taking into account (i) convective amplification due to the motion of the elementary sound sources, (ii) geometrical spreading, (iii) atmospheric attenuation, (iv) refraction and ground effects
- Energetic summation of the sound pressures from all elementary sources at listener position

Overall objective of this work is assessing the effect of aeroacoustically relevant blade modifications on a wind turbine's far field acoustics. As a first step, in this paper a few semi-analytical sub-models from literature for the sources, their directivity and the effect of source motion are compiled and integrated into a wind turbine sound prediction tool. Due to complexity, atmospheric damping, ground-effects and refraction are neglected for the time being. Eventually, in a preliminary case study, the tool is applied to tackle the problem, how the sound from wind turbine blades is modified by source delocalisation due to blade elasticity.

2. Sub-models from literature and synthesis

2.1 Trailing edge sound source model

The so-called trailing edge sound results from the interaction of the turbulent boundary layer in the trailing edge region of an airfoil with its trailing edge. It has been subject of many investigations. BROOKS et al. [9] performed an extensive measurement campaign on NACA-0012 airfoils in an aeroacoustic wind tunnel and developed a semi-analytical model for the trailing edge sound, in principle based on the theory by FFOWCS WILLIAMS and HALL [10]. Their model predicts the 1/3 octave band spectrum of the sound pressure level SPL_{TOT} around the trailing edge as a function of boundary layer displacement thickness δ^*, angle of attack α, free mach number M of the airfoil, the spanwise length L of the blade segment, the distance r between the source and the observer, the directivity function $D_{SCHLINKER}$ according to SCHLINKER and AMIET [11], and different correction factors A, B, K_1, K_2 and ΔK_1. The total turbulent boundary layer trailing edge sound comprises three terms

$$SPL_{TOT} = 10\log\left(10^{SPL_\alpha/10} + 10^{SPL_s/10} + 10^{SPL_p/10}\right) \text{ [dB]}, \qquad (1)$$

where SPL_α contains the scaling model for the angle of attack α

$$SPL_\alpha = 10\log\left(\frac{\delta_S^* M^5 L D_{SCHLINKER}}{r^2}\right) + B\left(\frac{St_s}{St_2(\alpha)}\right) + K_2(\alpha) \quad \text{[dB]}, \tag{2}$$

and SPL_p and SPL_S are the contributions from the pressure (p) and suction (s) side of the airfoil:

$$SPL_p = 10\log\left(\frac{\delta_p^* M^5 L D_{SCHLINKER}}{r^2}\right) + A\left(\frac{St_p}{St_1}\right) + (K_1 - 3) + \Delta K_1 \quad \text{[dB]} \tag{3}$$

$$SPL_s = 10\log\left(\frac{\delta_s^* M^5 L D_{SCHLINKER}}{r^2}\right) + A\left(\frac{St_s}{St_1}\right) + (K_1 - 3) \quad \text{[dB]} \tag{4}$$

The Strouhal numbers for the pressure and suction side are

$$St_p = \frac{f\delta_p^*}{U},\ St_s = \frac{f\delta_s^*}{U} \tag{5, 6}$$

where f is the acoustic frequency and U is the free-stream velocity. St_1 is a function of Mach number M only:

$$St_1 = 0{,}02 \cdot M^{-0{,}6} \tag{7}$$

St_2 depends on St_1 and α:

$$St_2 = St_1 \cdot \begin{cases} 1 & (\alpha < 1{,}33°) \\ 10^{0{,}0054(\alpha - 1{,}33)^2} & (1{,}33° \le \alpha \le 12{,}5°) \\ 4{,}72 & (12{,}5° < \alpha) \end{cases} \tag{8}$$

The resulting point source is located in the centre of the trailing edge of the blade segment.

The directivity function of the point source is a key component in the model. Originally it has been derived by SCHLINKER and AMIET [11] as

$$D_{SCHLINKER} = 2 \cdot \sin^2\left(\frac{\Theta_A}{2}\right) \cdot \sin^2(\Phi_A). \tag{9}$$

The definitions of the angles between the trailing edge sound source and the observer are given in **Fig. 2**. The distance between the observer and the sound source is named r. This function is frequency-independent and normalized such that $D_{SCHLINKER}(\Phi_A = \Theta_A = 90°) = 1$.

Two alternative frequency-independent directivity functions for trailing edge sound have been reported:

$$D_{HOWE} = 2 \cdot \sin^2\left(\frac{\Theta_H}{2}\right) \cdot \sin(\Phi_H) \tag{10}$$

(HOWE [12] or KAMBE et al. [13], D_{HOWE} ($\Phi_H = \Theta_H = 90°$) = 1), and

$$D_{OERLEMANS} = \left[2 \cdot \sin^2\left(\frac{\Theta_A}{2}\right) \cdot \sin^2\left(\Phi_A\right) \right]_{\Delta\beta,\Delta\gamma-averaged} \tag{11}$$

(OERLEMANS and SCHEPERS [14], $D_{OERLEMANS}$ ($\Phi_A = \Theta_A = 90°$) = 1). The latter is basically a modification of SCHLINKER's directivity function. Based on experimental results OERLEMANS and SCHEPERS applied an averaging over β and γ_R: "($d\beta$, $d\gamma_R$) is chosen to be ($\pi/12$, $2\pi/3$) for $\beta = 0°$, and is reduced to (0,0) for $\beta = \pi/2$ (using the error function)" [14]. All those directivity functions are visualized in **Fig. 3**.

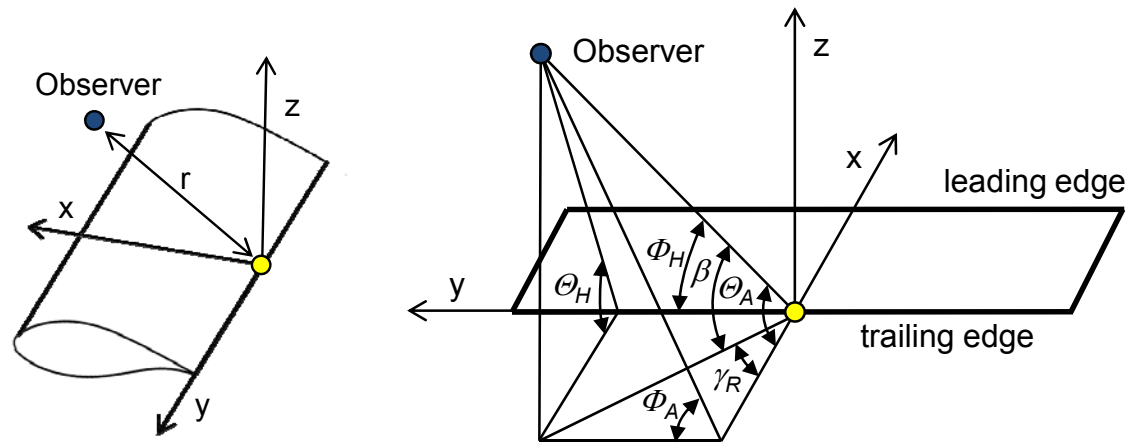

Figure 2: Definition of angles between trailing edge source and observer according to KAMBE et al. [13] , HOWE [12] and SCHLINKER and AMIET [11]

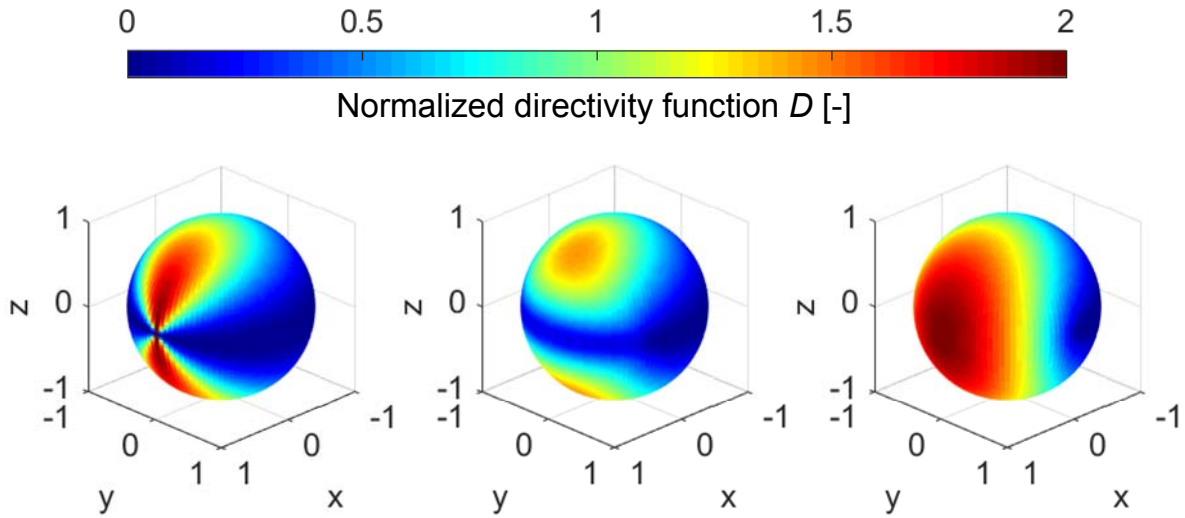

Figure 3: Visualisation of the directivity functions (from left to right): $D_{SCHLINKER}$, $D_{OERLEMANS}$ and D_{HOWE}; after OERLEMANS and SCHEPERS [14].

Another popular trailing edge sound source model for the far-field sound is due to AMIET [15]. In contrast to the previous models it is frequency-dependent and requires the surface pressure fluctuations on the airfoil as an input. However, MOREAU and ROGER [16] have shown that for low mach numbers ($M < 0.3$) and aocustic compact radiators ($C/\lambda >> 1$) AMIET's directivity function approaches HOWE's [12]. These criterions are met at the outer part of the blades of modern wind turbines where the mach number is around $M = 0.2$ according to OERLEMANS [17] and the trailing edge sound has its spectral peak at $C/\lambda > 10$ according to BROOKS et al. [9].

2.2 Moving sound sources

As described by many authors such as ROZENBERG et al. [18], SINAYOKO et al. [19] or CRIGHTON et al. [20], the motion of a sound source relative to the observer has an influence on the perceived mean square value of the sound pressure and the spectral shape of the sound (in the far-field). A simple explanation for this phenomenon of the so-called convective amplification is due to ROZENBERG et al. [18]: When the sound source moves towards the observer, the distance and therefore the travelling time of the acoustic energy to the observer is reduced. Hence, the observer receives the same acoustic energy from the source but in a shorter time which is equivalent to an increase of acoustic power (mean square value of the sound pressure).The convective amplification factor

$$CA = \frac{S'_{pp}}{S_{pp}} = \frac{1}{\left(1 - M_{SO}\right)^n} \tag{12}$$

represents the relationship between the power spectral density of the sound pressure at the source S_{pp} and at the observer S'_{pp}. Assuming CA being independent of frequency, this convective amplification factor also holds true for the overall sound pressure level (*OASPL*). The various amplification-factors found in the literature differ exclusively in the value of the exponent n. The derivation by ROZENBERG et al. [18] is based on the principle of energy conservation and yields an exponent $n = 1$. Starting with a different ansatz, SINAYOKO et al. [19] came up with an exponent of $n = 2$. Other derivations of the convective amplification are based on the inhomogeneous wave equation which describes the spreading of waves in fluids. By inserting different source-terms, it is possible to investigate the effect of motion for different sound sources. GOLDSTEIN [21] as well CRIGHTON et al. [20] inserted volume and mass point sources and came up with an exponent $n = 4$.

2.3 Geometrical considerations

The directivity function angles Θ_A, Θ_H, Φ_A, Φ_H are depicted in **Fig. 4**. The source S, observer O and hub H are shown and the angles of the directivity functions are marked according to HOWE [12], KAMBE et al. [13] and SCHLINKER and AMIET [11]. Therefore, an oblique pyramid is spanned between the source and observer with its base point on an edge of the base area. The base area is defined by the span-wise and chord-wise direction vectors at the point S which depend on the stagger and cone angles. After that, the points P_{BP}, P_2 and P_3 can be calculated. The scalar product is then used to determine the desired angles.

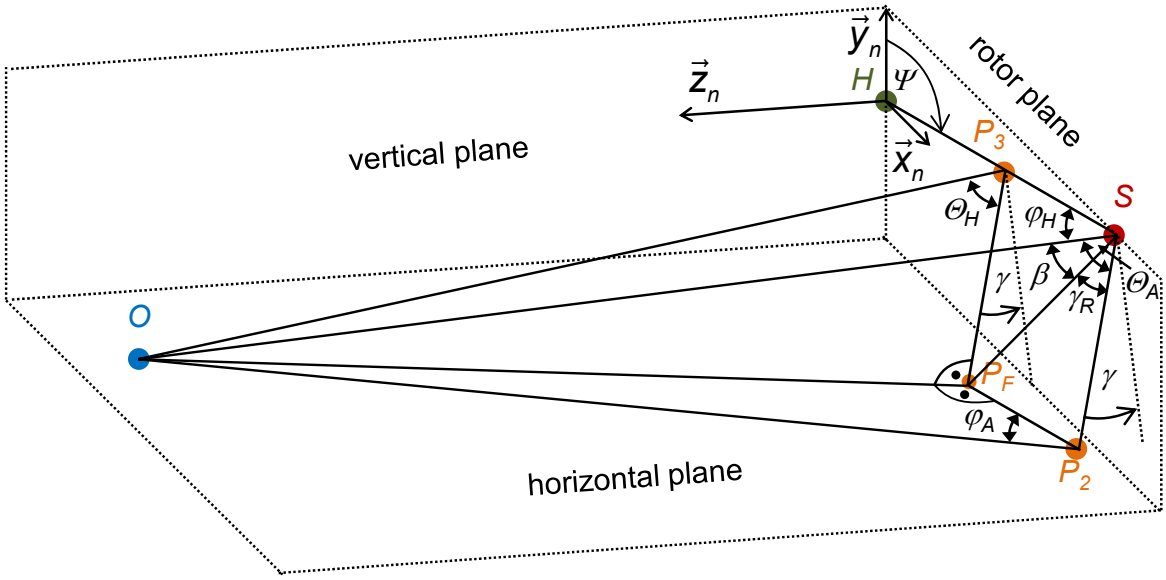

Figure 4: Definition of the directivity function angles Θ_A, Θ_H, Φ_A, Φ_H according to HOWE [12], KAMBE et al. [13] and SCHLINKER and AMIET [11].

The cross section of a blade element is shown in **Fig. 5** which moves in the plane of rotation with the circumferential speed of $-v_r$ from right to left. The direction of the wind is from bottom to top and therefore the relative inflow velocity W_∞ points from bottom left to top right. The definitions of the angle of attack α, the free inflow angle β_∞ and the stagger angle γ are depicted in **Fig. 5** as well. The stagger angle γ is the sum of the rotor twist angle σ_R, the pitch angle σ_P and the elastic torsion angle σ_T.

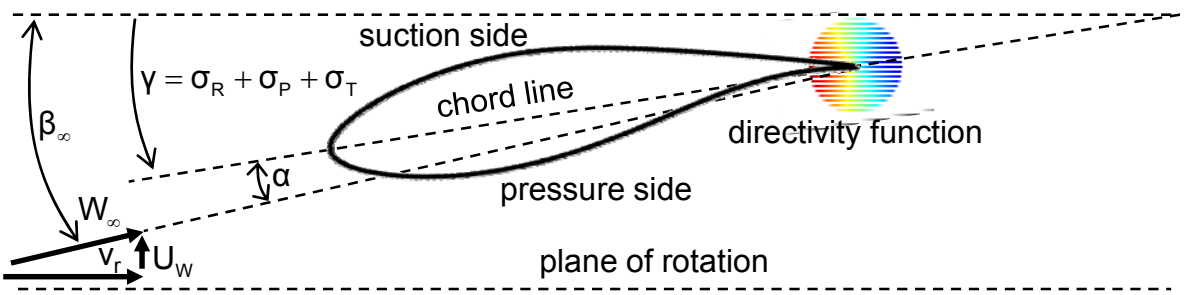

Figure 5: Cross section of a blade element with speed triangle and resulting angles.

The rotor twist angle σ_R is the manufactured twist of the blades and therefore fixed during operation. In contrast, the pitch angle σ_P may be adjusted during operation in order to control the power output of the wind turbine. Finally, the elastic torsion angle σ_T describes the elastic deformation of the rotor blades during the operation and depends on the wind load. In **Fig. 6** a schematic diagram of a sound source on the wind turbine and some more relevant angles can be seen. The azimuth angle Ψ describes the circumferential position of the source, the stagger angle γ represents the overall rotational angle of the source around the blade radius, while the tilt angle Γ_W shows the tilt of the nacelle relative to the horizon and the cone angle β_{cone} describes the angle between the blade radius and the rotation plane.

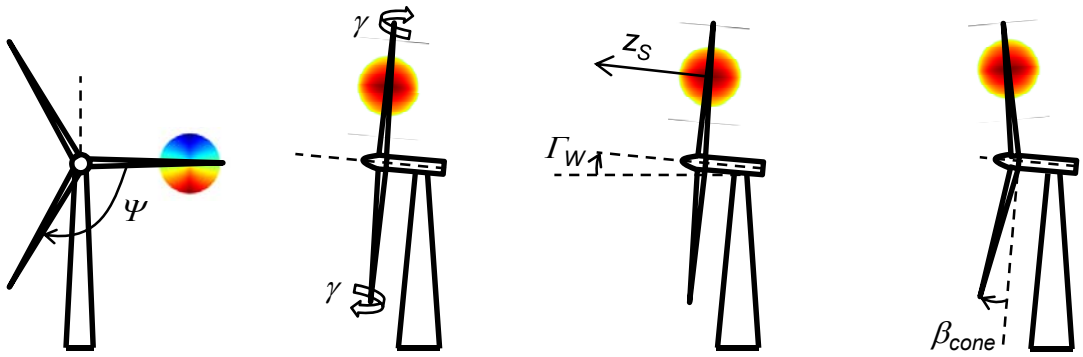

Figure 6: Schematic illustration of a point sound source on a wind turbine blade and the resulting angles.

2.4 Synthesis

In analogy to BOORSMA and SCHEPERS [22] and OERLEMANS and SCHEPERS [14] the sub-models are compiled into one tool. The sound pressure level due to sound radiated by a particular point source, received by a observer at observer time instance *t'*, becomes

$$SPL_{1/3}\left(r,\ \Phi_A,\ \Theta_A;\ f',\ t'\right) = \left\{ SPL_{TOT,ref}\left(f\right) + 10\log\left(D\left(\Phi_A,\ \Theta_A\right)\right) + 10\log\left(CA\left(M_{SO}\right)\right) - 10\log\left(\frac{r}{r_{ref}}\right)^2 \right\}\Bigg|_t \quad \text{[dB]} \tag{13}$$

(here in terms of 1/3 octave bands), with

$$SPL_{TOT,ref}\left(f\right) = SPL_{TOT}\left(r_{ref} = 1\ \text{m},\ \Phi_A = \Theta_A = 90°;\ f\right) \quad \text{[dB]} \tag{14}$$

and the Doppler shifted frequency [23]

$$f' = f \cdot \left(1 - M_{SO}\right)^{-1}. \tag{15}$$

The sound pressure spectrum $SPL_{1/3}(r,\ \Phi_A,\ \Theta_A;\ f',\ t')$ belongs to a small time interval in which the motion of the sound source can be regarded as approximately linear with respect to the observer. (When using HOWE's directivity function, the angles Φ_A, Θ_A are replaced by Φ_H, Θ_H.) Having substituted the sound radiating wind turbine blades by *m* sound sources, each sound source has its own M_{SO} (in *CA*) as well as *r*, $SPL_{TOT,ref}$ and *D*. The overall sound pressure level from one sound source as seen by the observer then becomes

$$OASPL_{source}\left(t'\right) = 10\log\left(\frac{\int_0^\infty SPL_{1/3}(t',f')df'}{p_{ref}^2}\right) \quad \text{[dB]}. \tag{16}$$

Since each $OASPL_{source}$ arrives at the observer at its individual retarded time instance

$$t' = t + \frac{r}{c}, \tag{17}$$

a resampling with respect to t' within one rotor revolution is required to obtain values at a common time base. Eventually, the overall sound pressure level *OASPL* from all *m* moving sources as a function of t' is obtained as

$$OASPL(t') = 10\log\sum_{i=1}^{m} 10^{\frac{OASPL_{source,i}(t')}{10}} \quad \text{[dB]}. \tag{18}$$

Hereby we assumed that the sound sources (here trailing edge sound sources) radiate incoherently.

To further analyse the time dependent *OASPL*, the equivalent overall sound pressure level

$$OASPL_{eq} = 10\log\left(\frac{1}{T}\int_{t_0}^{t_0+T} 10^{\frac{OASPL(t')}{10}} dt'\right) \quad \text{[dB]} \tag{19}$$

and the amplitude modulation

$$OASPL_{am} = \max\left(OASPL(t')\right)\Big|_T - \min\left(OASPL(t')\right)\Big|_T \quad \text{[dB]} \tag{20}$$

are introduced. Both are calculated over one period of revolution *T*.

The steps of the combined sound prediction model, as implemented in a MatLab™ code, are shown in **Fig. 7**. Inputs are the wind turbine parameters and the positions of the sound sources along the blades are defined and the observer points fixed. Then, the angles Φ_A, Φ_H, Θ_A, Θ_H, the Mach number M_{SO} and the retarded time t' for every source-observer-combination are derived. In a next step, the directivity factor *D* and convective amplification factor *CA* for every source-observer-combination and the boundary layer displacement thickness on the suction δ_s and the pressure side δ_p for every blade segment are calculated with XFOIL. Based on the boundary layer information, the model by BROOKS et al. [9] (BPM-model) is used to calculate the $SPL_{TOT,ref}$ for every sound source. Then, at discrete time instances the sound immission on the observer points are calculated. Finally, the immission is resampled with respect to t' within one rotor revolution to obtain values at a common time base and all sound sources are superpositioned at the observer points.

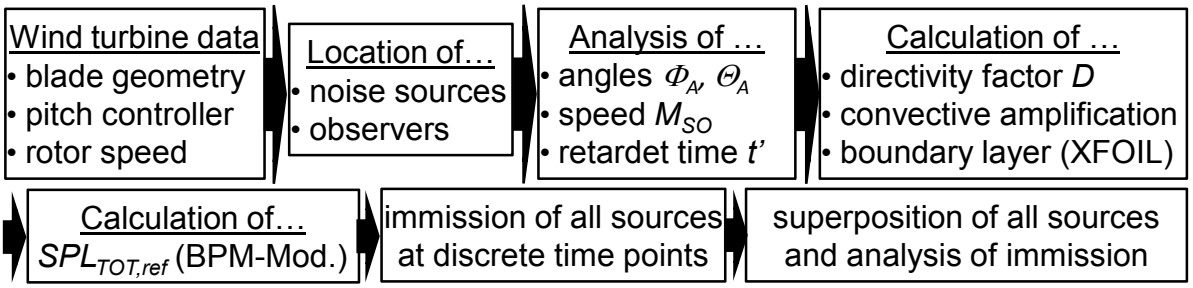

Figure 7: Structure of the sound prediction model.

In contrast to BOORSMA and SCHEPERS [22] and OERLEMANS and SCHEPERS [14] we here implement all three different directivity functions and the three amplification factors in order to assess the impact of the model choice on the results.

3. Case study

3.1 Benchmark turbine

Since published data are rare, we take - as a first benchmark - the horizontal axis wind turbine as investigated by OERLEMANS and SCHEPERS [14]. It has a rotor half diameter of 47 m and a hub height of 100 m. In OERLEMAN et al.'s paper the free field wind speed is between 6 - 8 m/s. Here we assume a fixed value of 7 m/s.

Since not all parameters of this turbine have been published we more or less arbitrarily estimate other required parameters: The blade varies linearly from 3.5 m at the hub to 0.8 m at the tip. A DU93W210TET03 blade profile is assumed where TET03 indicates a trailing edge thickness of 0.3% of chord length. The rotational speed is set to 11.6 rpm. Within the case study, the angle of attack is fixed to α = 6° = const. along the complete span. Tilt and pitch angle (Γ_W, σ_P) are set to 0° as well as torsion and cone (σ_T, β_{cone}) angle in the case of rigid blades.

With this basic setup and with the known free inflow angle β_∞, the rotor twist angle σ_R and the stagger angle γ can be calculated for all blade segments. In the case of elastic deformed rotor blades, the rotor twist angle of the rigid blades combined with an assumed elastic torsion according to **Fig. 8** is used to calculate the new stagger angle and new angle of attack.

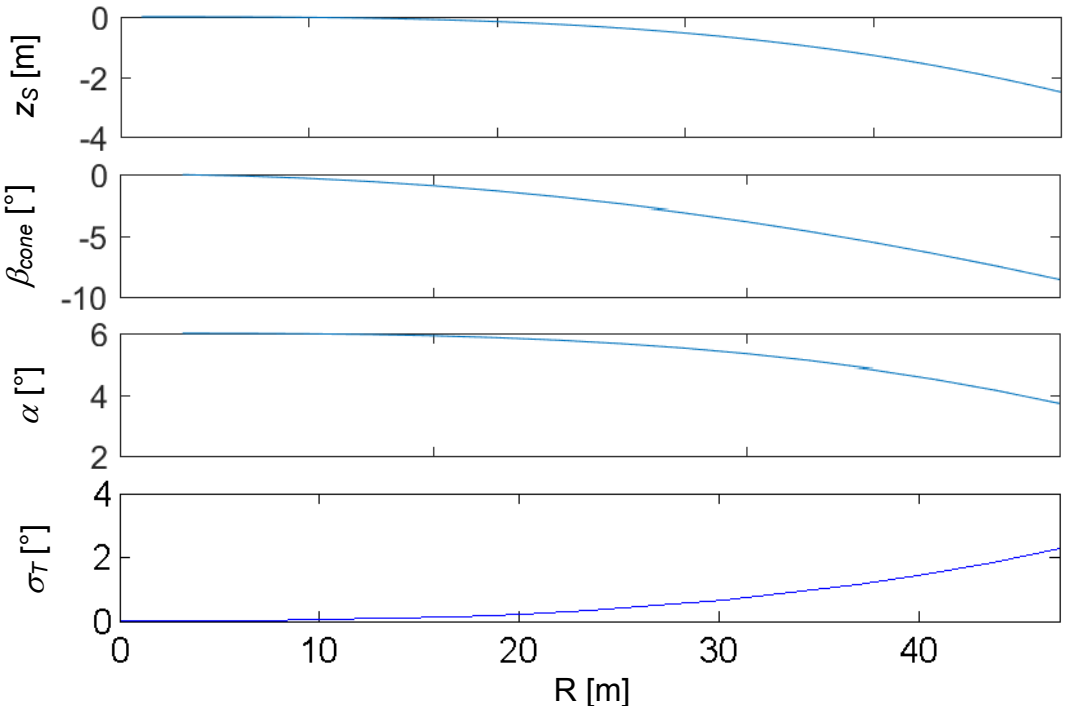

Figure 8: Assumed bending line z_S, cone angle β_{cone}, angle of attack α and elastic torsion angle σ_T in the case of elastic deformation drawn as a function of the blade radius.

For considering elasticity of the blades, we assume a bending line z_S, a cone angle β_{cone}, a resulting angle of attack α and the elastic torsion angle σ_T as in **Fig. 8**. The assumed deformation of the wind turbine blade is shown in **Fig. 9**; the location of the sound sources is also indicated.

In this case study, the time resolutions obtained is due to 40 spatial rotor-positions (i.e. time instances) considered within one rotor revolution.

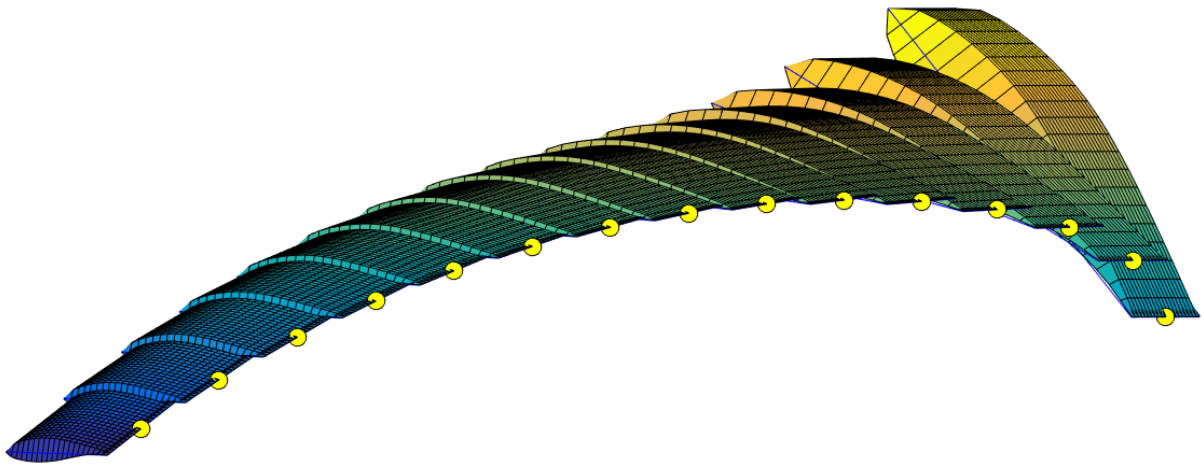

Figure 9: Segmentation of the elastically deformed wind turbine blade and positions of the trailing edge sound sources (yellow spheres).

3.2 Results

3.2.1 Turbine with rigid blades: General radiation characteristic

As an example, we present the radiation characteristic of the benchmark turbine with completely rigid blades as predicted utilizing directivity function and convective amplification factor D_{HOWE} and $CA_{Rozenberg}$, respectively. In **Fig. 10**, the observer positions on a circle around the wind turbine are schematically shown expressed in terms of observer angle ζ and distance from foot to observer r_{Obs} (left) and the *OASPL* as a function of the observer time *t'* within one rotor revolution for three different observer positions ζ = 0°, 63°, 90° is shown schematically. The circle has a diameter of 120 m on the ground around the foot of the wind turbine, i.e. r_{Obs} = 60 m. The observer angle ζ is 0° in front and 180° at the back of the turbine. The swishing character of the wind turbine sound can be seen very well - particularly at the side of the wind turbine (ζ = 90°).

In **Fig. 11**, the equivalent overall sound pressure level $OASPL_{eq}(\zeta)$ (left) and the amplitude modulation $OASPL_{am}(\zeta)$ (right) for 81 observers around the wind turbine is shown. The highest equivalent $OASPL_{eq}$ are found at ζ = 0° and ζ = 180°, the lowest at ζ = 90° and ζ = 270°. The amplitude modulation is very significant at ζ = 90° and ζ = 270° and close to zero at ζ = 0° and ζ = 180°. This is only a qualitative analysis, the absolute levels can not be validated at this time of the project.

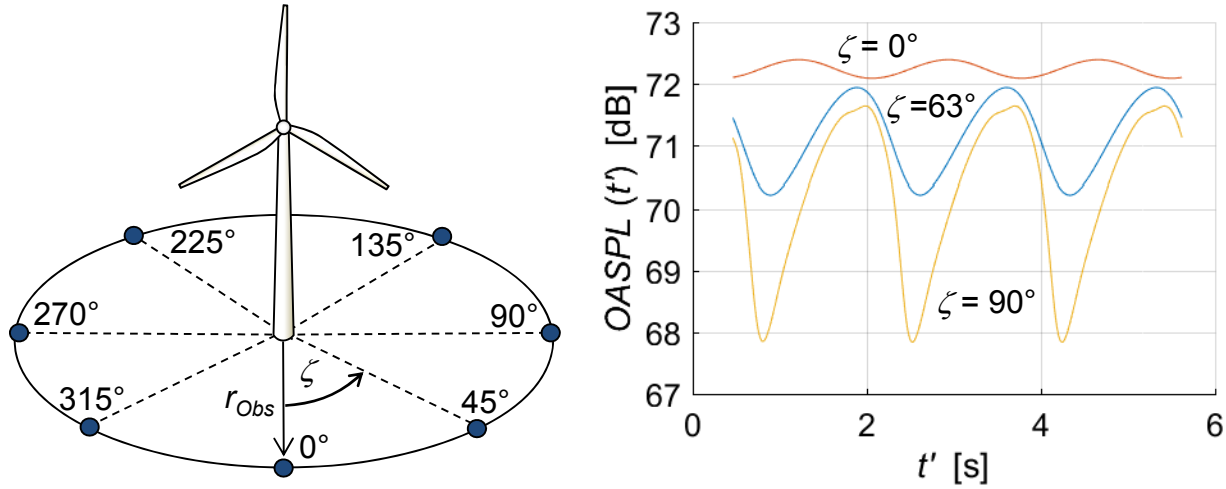

Figure 10: Observer positions in a circle around the wind turbine as a function of the observer angle ζ (left) and *OASPL*(*t'*) within one rotor revolution for three different observer positions ζ = 0°, 63°, 90° at r_{Obs} = 60 m - utilizing D_{HOWE} and $CA_{Rozenberg}$

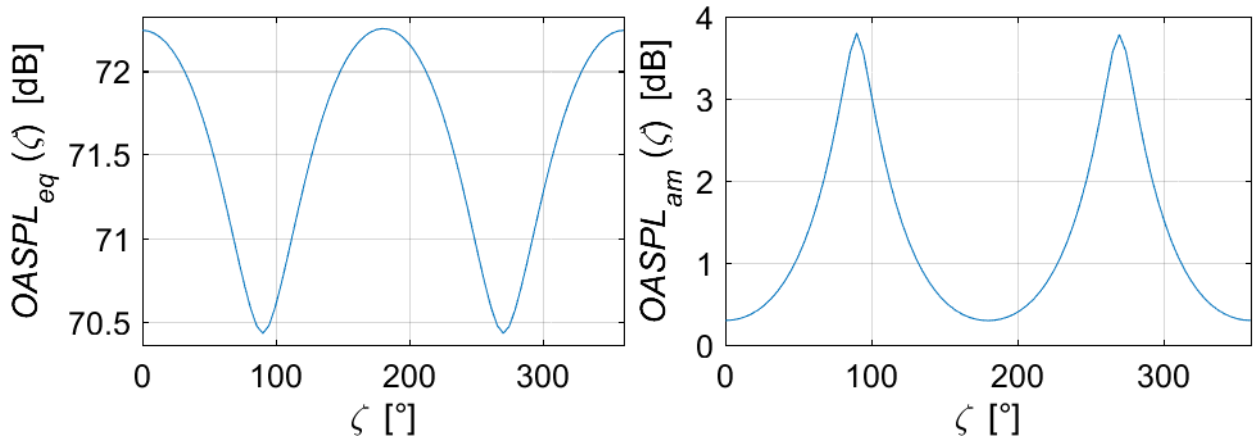

Figure 11: Equivalent overall sound pressure level $OASPL_{eq}(\zeta)$ (left) and amplitude modulation $OASPL_{am}(\zeta)$ (right) at r_{Obs} = 60 m around the wind turbine - utilizing D_{HOWE} and $CA_{Rozenberg}$

3.3.2 Effect of choice of sub-models

The different trailing edge sound directivity functions have a major impact on the predicted overall sound pressure level (*OASPL*) at the observer points. Because OERLEMANS and SCHEPERS [14] documented normalized measurement data, all simulation results are also normalized with respect to the observer position directly in front of the wind turbine:

$$OASPL_{eq,norm}(\zeta) = OASPL_{eq}(\zeta) - OASPL_{eq}(\zeta = 0°) \quad \text{[dB]} \tag{21}$$

$$OASPL_{am,norm}(\zeta) = OASPL_{am}(\zeta) - OASPL_{am}(\zeta = 0°) \quad \text{[dB]} \tag{22}$$

For the same case as in section 3.3.1 it can be seen from **Fig. 12** that the immission for all directivity functions is very similar directly in front of (ζ = 0°) and behind (ζ = 180°) the wind turbine. Moreover, it becomes clear that the highest immission is directly up- and downstream of the wind turbine. The major differences due to the directivity functions chosen are observed at the sides of the wind turbine (ζ = 90° and 270°). The directivity functions $D_{OERLEMANS}$ and $D_{SCHLINKER}$ cause a pronounced directivity pattern of $OASPL_{eq,norm}$ (with a variation up to 11 dB and 18 dB, respectively) whereas with D_{HOWE} the directivity is nearly level.

The normalized amplitude modulation $OASPL_{am,norm}$ (**Fig. 12**, lower diagram) is minimal directly in front and behind of the turbine. At the turbine sides, the highest normalized amplitude modulation and the largest impact of the directivity functions chosen can be seen. The directivity function $D_{SCHLINKER}$ predicts over 50 dB of normalized amplitude modulation, whereas with $D_{OERLEMANS}$ and D_{HOWE} approximately 4 dB are predicted. As initially mentioned OERLEMANS and SCHEPERS [14] published experimental data, which are plotted in **Fig. 12** as well. Obviously, utilizing the directivity function D_{HOWE} in our prediction scheme yields results which come closest to OERLEMANS' experimental data.

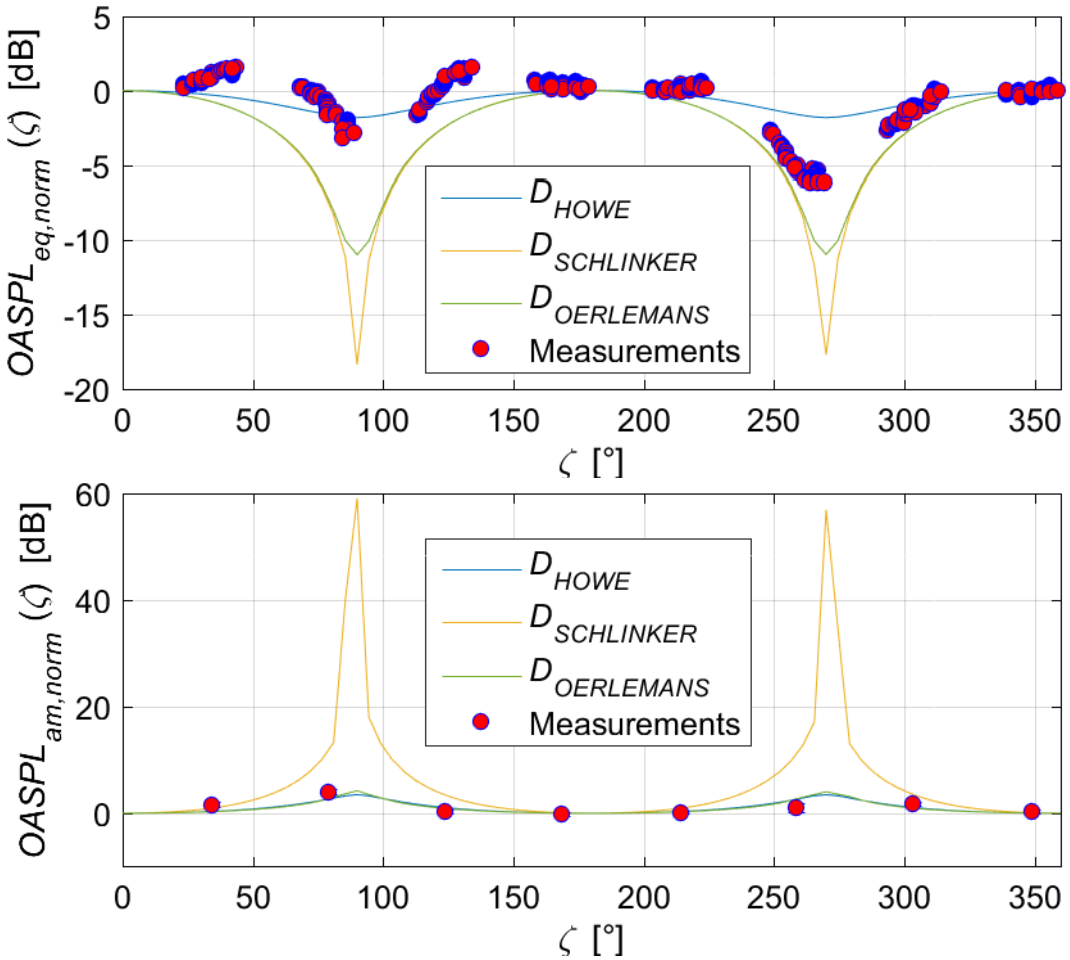

Figure 12: Effect of the directivity sub-models on the normalized equivalent $OASPL_{eq,norm}$ (upper diagram) and the normalized amplitude modulation $OASPL_{am,norm}$ (lower diagram) for observer positions in a circle around the wind turbine at r_{Obs} = 60 m. Experimental data from OERLEMANS and SCHEPERS [14].

Another more fundamental experiment reported in the literature confirmed this finding. KAMBE et al. [13] validated experimentally HOWE's directivity function for a flat plate rather an airfoil. They generated eddies with a radius of 4.7 mm and sent them over the edge of a plate (M = 0.1 to 0.2, C = 1 m). The major advantage of this experiment was its reproducibility and the absence of any superimposed flow. In consequence, KAMBE et al. [13] was able to measure the sound pressure at 70 positions in a plane normal to the surface and along the cord line and in a plane parallel to the surface in an angular range from 0° to 360°. **Fig. 13** depicts the measured sound pressure amplitudes and the predicted with HOWE's model in the plane normal to the surface of the plate and along the cord line (left) and in a plane parallel to the surface (right). It can be seen that HOWE's directivity function agrees very well with the measurements and only small differences were found.

The directivity functions $D_{SCHLINKER}$ and $D_{OERLEMANS}$ are inconsistent with the measurement results from KAMBE et al. [13] because they are zero on the surface of the plate. Therefore, again HOWE's directivity function seems to be the most plausible.

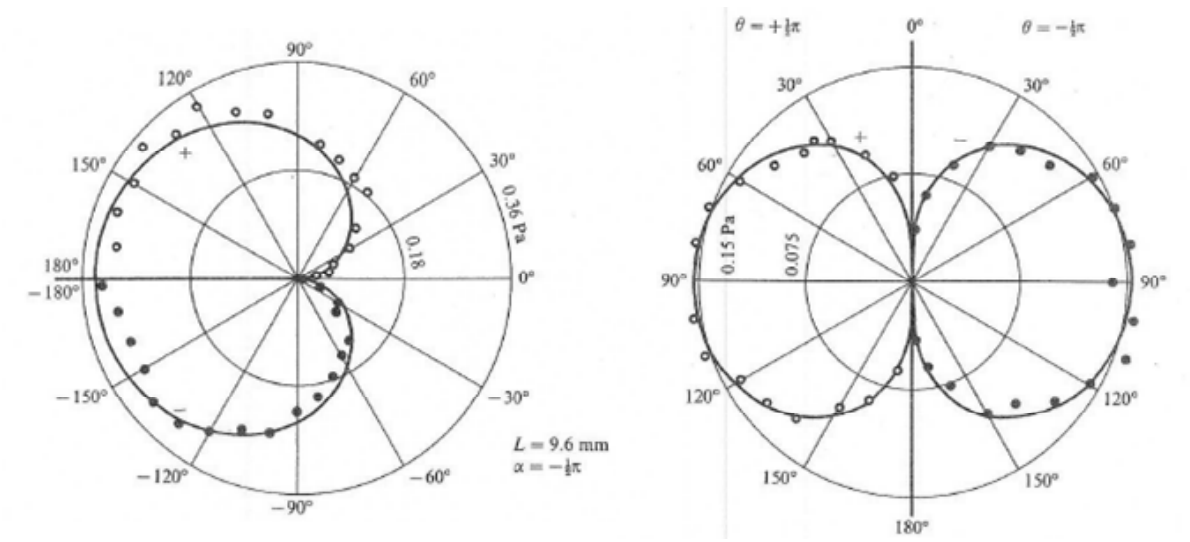

Figure 13: Trailing edge sound: Directivity of sound pressure amplitudes in a plane normal to the surface of the flat plate and along the cord line (left) and in a plane parallel to the surface (right); HOWE's prediction (solid line) and experimental data (circles) by KAMBE et al.; from KAMBE et al. [13] .

The impact of the different convective amplification sub-models on the predicted $OASPL_{eq,norm}$ and $OASPL_{am,norm}$ can be seen in **Fig. 14.** Here we use the sub-model D_{HOWE}. The greatest impact is found at ζ = 90° and 270° but compared to the choice of D it is comparably small. Hence, the convective amplification sub-model $CA_{Rozenberg}$ is chosen for a consistent prediction model since it satisfies the conservation of acoustic energy.

3.3.3 Effect of elastic blade deformation

To investigate the influence of the elastic deformation of the rotor blades we exclusively utilize the sub-models D_{HOWE} and $CA_{Rozenberg}$. **Fig. 15** compares the sound immitted at the obervers points from the rigid and elastic blade. It can be seen that the differences are smaller than 0.5 dB, hence negligible.

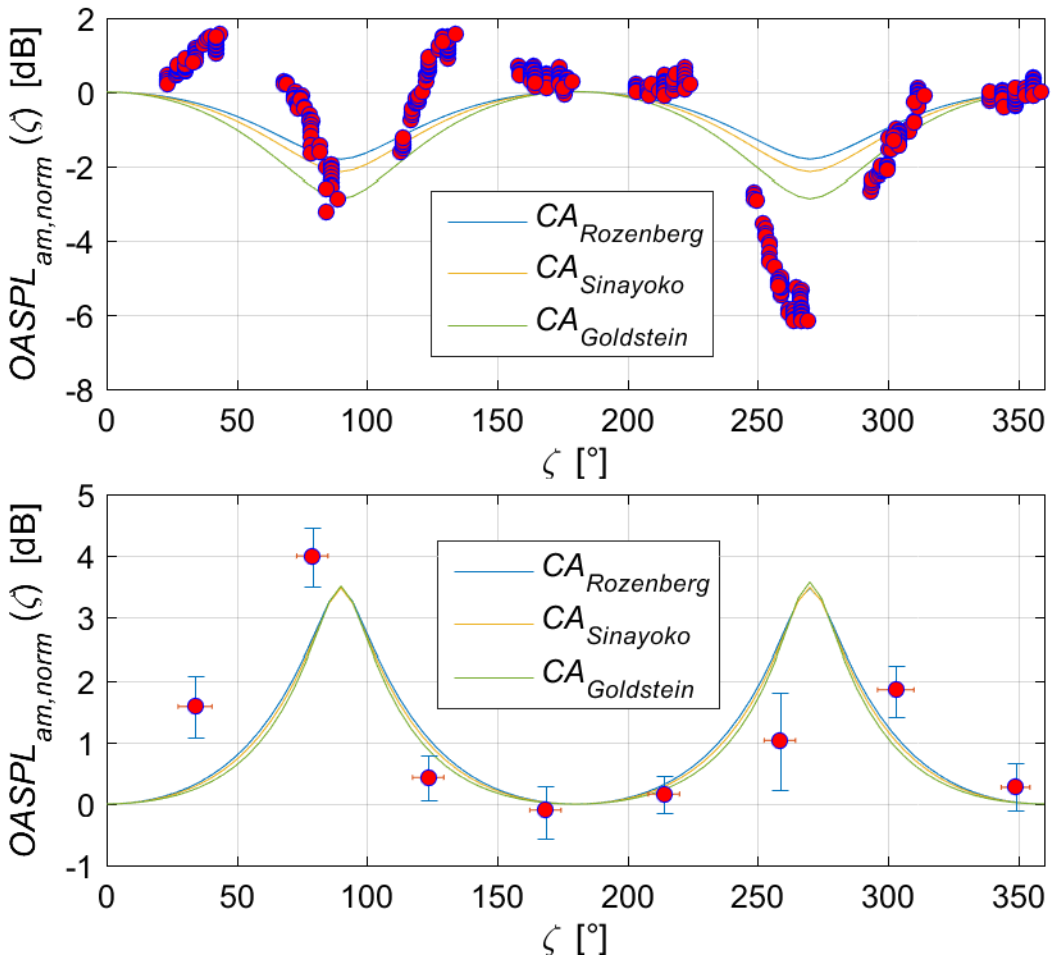

Figure 14: Effect of the convective amplification sub-models on the normalized equivalent $OASPL_{eq,norm}$ (upper diagram) and the normalized amplitude modulation $OASPL_{am,norm}$ (lower diagram) for observer positions in a circle around the wind turbine at r_{Obs} = 60 m. Experimental data from OERLEMANS and SCHEPERS [14].

4. Summary and Conclusions

The objective of this paper was to compile and compare selected aeroacoustic semi-analytical wind turbine sound prediction models available in the open literature.

The general structure of those models is found to be similar: A combination of sub-models for the elementary sound sources on the blades and a sound propagation model from the sources to the listener. However, the sub-models found in the literature vary and an thorough assessment based on experiments is not an easy task.

The predicted *OASPL* around a wind turbine is shown to be affected substantially by the choice of the modelled directivity function of the elementary point sources representing the full blades. Given three simple, frequency-independent directivity functions ($D_{SCHLINKER}$, $D_{OERLEMANS}$ and D_{HOWE}) HOWE's source directivity function seems to yield results, that match best with experimental results from literature.

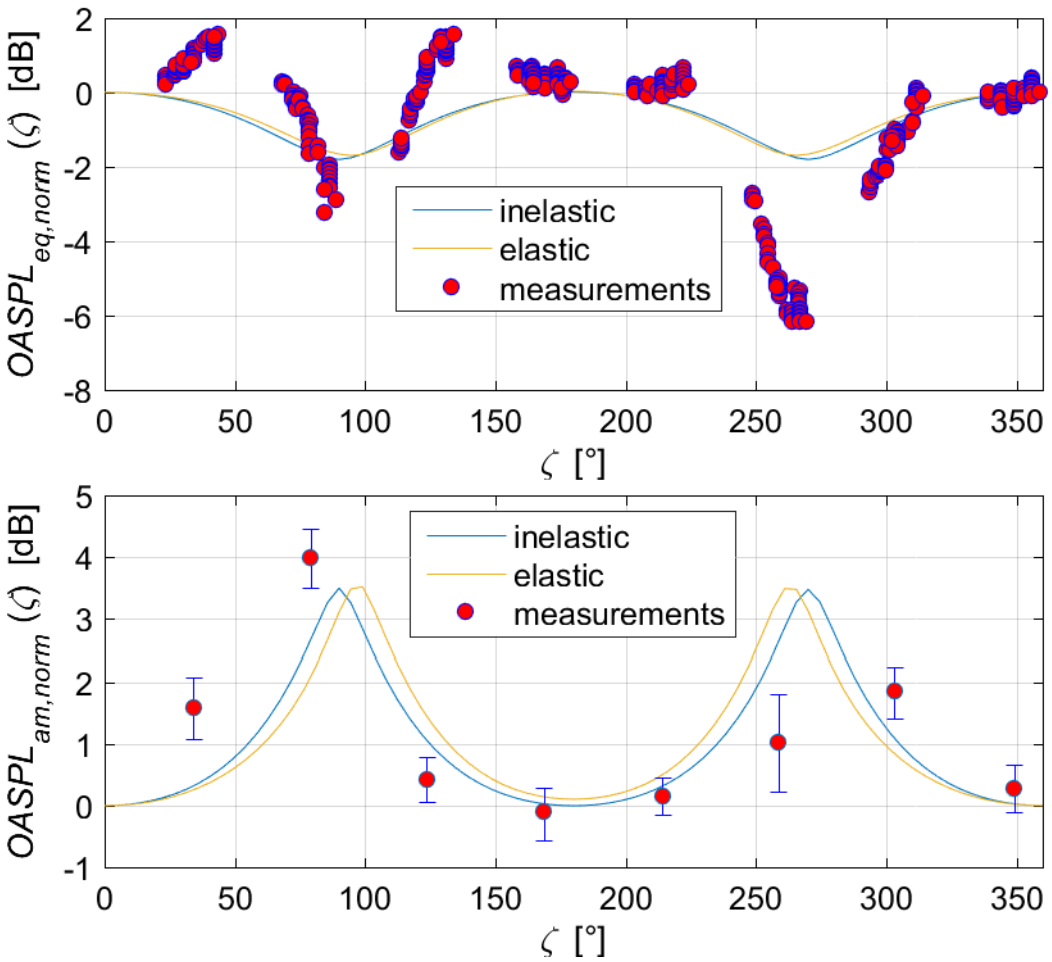

Figure 15: Effect of the elastic deformation of the rotor blades on $OASPL_{eq,norm}$ and $OASPL_{am,norm}$ at r_{Obs} = 60 m - sub-models from $CA_{Rozenberg}$ and D_{HOWE}**.** Experimental data from OERLEMANS and SCHEPERS [14].

The effect of the models which take into account the motion of the sound sources is significantly smaller as compared to the source models. Three models for the convective amplification factors ($CA_{ROZENBERG}$, $CA_{SINAYOKO}$ and $CA_{CRIGHTON}$) where compared. From principle considerations ROZENBERG's approach seems to be the most consisting.

Eventually, combining selected sub-models, a preliminary own wind turbine sound prediction model was compiled and encoded, yielding the acoustic footprint of the turbine on ground level and the swishing character of the wind turbine sound.

In a first case study, the effect of delocalisation of elementary sound sources along the blades and a modification of the local angle of attack due to the flexibility of the blade has been studied. As a preliminary result, the effect of blade elasticity on the acoustic emission of a complete wind turbine rotor seems to be small when comparing to a rigid rotor. It is important to note that so far the atmospheric attenuation, refraction and ground effects have not been taken into account - this remains for future studies and may affect these results.

Acknowledgement

This work has been funded by the Bundesministerium für Wirtschaft und Energie (Federal Ministry for Economic Affairs and Energy) of Germany within the project RENEW (FKZ 0325838B).

References

[1] EGGENSCHWILER, K.; HEUTSCHI, K.;SCHÄFFER, B.; PIEREN, R.; BÖGLI, H.; BÄRLOCHER, M.; Wirkung und Beurteilung des Lärms von Windenergieanlagen, Lärmbekämpfung, Springer VDI Verlag, 2016 (Nr. 5, pp. 159-167)

[2] LUTZ, T. ; ARNOLD, B. ; WOLF, A. ; KRÄMER, E.: *Numerical Studies on a Rotor with Distributed Suction for Noise Reduction,* TORQUE 2014, Journal of Physics: Conference Series 524, 2014

[3] GERHARD, T. ; ERBSLÖH, S. ; CAROLUS, T.: *An Experimental and Numerical Parameter Study on Trailing Edge Blowing for Reduced Trailing Edge Noise,* 6th International Conference on Wind Turbine Noise, Glasgow, 2015

[4] VATHYLAKIS, A. ; CHONG, T.P. ; PARUCHURI, C. ; JOSEPH, P.F.: *Sensitivity of Aerofoil Self Noise Reductions to Serration Flap Angles,* 22nd AIAA/CEAS Aeroacoustics Conference, France, 2016

[5] OERLEMANS, S.;SIJTSMA, P.; MÉNDEZ LÓPEZ, B.: Location and quantification of noise sources on a wind turbine, Journal of Sound and Vibration 299, 869-883, 2007

[6] LOWSON, M.V.: Assessment and Prediction of Wind Turbine Noise. Flow Solutions Report 92/19, ETSU W/13/00284/REP, pp. 1-59, Dec. 1992

[7] LIPS, W.:"Strömungsakustik in Theorie und Praxis: Anleitung zur lärmarmen Projektierung von Maschinen und Anlagen", Expert-*Verlag*, Renningen, 2008.

[8] DIN EN 61400-11 Windenergieanlagen - Teil 11: Schallmessverfahren (IEC 61400-11:2012); Deutsche Fassung EN 61400-11:2013

[9] BROOKS, T. F. ; POPE, D. S. ; MARCOLINI, M. A.: *Airfoil Self-Noise and Prediction*: *NASA RP-1218*. Hampton, Virginia : NASA Langley Research Center, 1989

[10] FFOWCS WILLIAMS, J. E., HALL, L. H.: Aerodynamic Sound Generation by Turbulent Flow in the Vicinity of a Scattering Half Plane, *Journal of Fluid Mechanics*, 1970 (40(4), pp. 657-670)

[11] SCHLINKER, R. H. ; AMIET, R.K.: *Helicopter rotor trailing edge noise*: *NASA Contractor Report 3470*, 1981

[12] HOWE, M. S.: *A Review of the Theory of Trailing Edge Noise*: Journal of Sound and Vibration, 1978 (61(3), pp. 1-145)

[13] KAMBE, T. ; MINOTA, T. ; IKUSHIMA, Y.: *Acoustic wave emitted by a vortex ring passing near the edge of a half-plane* : Journal of Fluid Mechanics, 1985 (Volume 155, pp. 77 - 103)

[14] OERLEMANS, S. ; SCHEPERS, J. G.: *Prediction of wind turbine noise and validation against experiment*. National Aerospace Laboratory NLR-TP-2009-402, 2009

[15] AMIET, R. K.: Noise due to turbulent flow past a trailing edge, Journal of Sound and Vibration, Vol. 47, No. 3, 1976, pp. 387-393.

[16] MOREAU, S. ; ROGER, M.: Back-scattering correction and further extensions of Amiert's trailing-edge noise model. Part II: Application, Journal of Sound and Vibration, 2009 (323, pp. 397-425)

[17] OERLEMANS, S.: Wind turbine noise: primary noise sources, National Aerospace Laboratory NLR-TP-2011-066, 2011

[18] ROZENBERG, Y. ; ROGER, M. ; MOREAU, S.: *Rotating blade trailing-edge noise: experimental validation of analytical model* : AIAA Journal, American Institute of Aeronautics and Astronautics, 2010 (48, pp. 951 - 962)
[19] SINAYOKO, S. ; KINGAN, M. ; AGARWAL, A.: *Trailing edge noise prediction for rotating blades: analysis and comparison of two classical approaches* : 33rd AIAA Aeroacoustics Conference, American Institute of Aeronautics and Astronautics, 2012
[20] CHRIGHTON, D. G. ; DOWNLING, A. P. ; FFOWCS WILLIAMS, J. E. ; HECKL, M. ; LEPPINGTON, F. G.: *Modern Methods in Analytical Acoustics*. 1. Auflage. Springer-Verlag, 1992
[21] GOLDSTEIN, M.: *Aeroacoustics*. USA: McGraw-Hill, 1976
[22] BOORSMA, K., SCHEPERS, J.G.: *Enhanced wind turbine noise prediction tool SILANT*: Wind Turbine Noise, 2011
[23] KUTTRUFF, H.: Akustik - Eine Einführung. Stuttgart : S. Hirzel Verlag, 2004